Bulk and surface properties of dispersed CuO phases in relation with activity of NO_x reduction

Simona Bennici, Paolo Carniti, and Antonella Gervasini*

Dipartimento di Chimica Fisica ed Elettrochimica, Università degli Studi di Milano, via Camillo Golgi, 19, I-20133 Milano, Italy

Received 7 June 2004; accepted 10 September 2004

Synthesized silicas modified with alumina, titania, and zirconia (about 13% wt) were used as supports for dispersing nanosized CuO phase. All the prepared catalysts, containing about 1 $mmol_{cu}\ g_{cat}^{-1}$, possessed high surface areas (230–430 $m^2\ g_{cat}^{-1}$) and homogeneous coverage of the relevant support, as revealed by SEM-EDS analysis. The nature of the support and its acidity directed the CuO deposition modifying the dimensions of the CuO aggregates and the ratio between highly and scarcely interacting copper species with support, as revealed by complementary analyses. The redox character of the CuO phase was studied realizing cycles of programmed temperature reduction/oxidation (TPR-TPO) which gave the extent of CuO reduction and Cu(O) re-oxidation. Deconvolution of the reduction profiles permitted identifying different copper species which presence depended on the support nature. Attempts were made to individuate relations between the properties of the CuO species and catalytic activity in NO_x reduction with ethene (HC-SCR process) in highly oxidant atmosphere. The CuO phase deposited on the most acidic supports showed the best activity and selectivity in the NO_x reduction.

KEY WORDS: copper oxide; silica supports; temperature-programmed-reduction; temperature-programmed-oxidation; NO_x reduction; HC-SCR.

1. Introduction

Copper oxide is among the most active transitional metal oxide catalysts for emission control reactions [1–5]. Catalysts based on finely divided copper oxide have displayed interesting activity towards total oxidation of CO, [6–8], hydrocarbons [6,9] and alcohols [10,11], and NO_x, and SO_2 reduction reactions [3–16]. In the case of selective catalytic reduction of nitrogen oxides (NO_x) by hydrocarbons in an oxygen-rich atmosphere, (HC-SCR process), various catalytic systems based on CuO dispersed with different methods on supports of different nature have been successfully reported in the literature [17–21].

To achieve high catalytic activity, it is necessary to highly disperse CuO particles in small aggregates on a support. By conventional methods for catalyst preparation, such as impregnation, inhomogeneous agglomeration of copper oxide species occurs especially at high copper content, and large-sized particles result [22,23]. Ion-exchange method, even if it is able to stabilize copper species assuring good dispersion, cannot be widely used because of the low loading of copper obtained due to the limit terminal –OH groups on the oxide surfaces. To obtain higher copper loading and stability of the copper species, grafting or chemisorption methods of deposition could be pursued [19,24]. Recently, our research group has used silica based oxides as supports for copper deposition by chemisorption–hydrolysis method [20], demonstrating its suitability in dispersing CuO in nanosized aggregates even for high copper loading (up to 9 wt% of CuO). Moreover, a suitable tailoring of CuO nanodomains that gave the highest and best activity and selectivity in the SCR of NO_x has been individuated (around 1.5–1.7 $atom_{Cu}\ nm^{-2}$) [21].

Besides the preparation method, the nature of the support plays a significant role in order to obtain well dispersed copper phase. For instance, the bad dispersion of the CuO phase for the CuO/SiO_2 system [20,25] could be related to the absence of acid sites on the support surface. It is then useful to select supports with controlled acidity able to stabilize the copper phase deposited on them avoiding copper sintering during the high temperature treatments, such as calcination, catalytic reaction, etc. The application of sol–gel chemistry to the preparation of mixed oxides has been largely pursued [26,27]. The sol–gel prepared mixed oxides approach homogeneity throughout the bulk at the molecular scale and show improved acidic properties, high surface area, and thermal stability [28,29]. Due to these properties, various synthesized mixed oxides have found application as catalysts or catalyst supports in chemical and petrochemical processes [30,31]. For example, silica-alumina is among the most used catalysts in catalytic cracking reactions and other acid catalysed reactions [21,32,33].

This work reports the characterization and catalytic activity of catalysts containing the dispersed CuO phase

*To whom correspondence should be addressed.
E-mail: antonella.gervasini@unimi.it

1011-372X/04/1200–0187/0 © 2004 Plenum Publishing Corporation

on modified silica oxides. The siliceous oxides containing Al, Ti, and Zr (silica–alumina (SA), silica–titania (ST), and silica–zirconia (SZ), respectively) were prepared by sol–gel route, their surface acidic characteristics have been presented elsewhere [34]. The copper phase was deposited on the support in an amount around 9 wt% as CuO by the chemisorption method that assured the finely dispersion of the CuO aggregates. Characterization of the obtained catalysts was aimed at controlling the red–ox properties and the distribution of the copper species as a function of the support nature. Catalyst activity was tested in the selective reduction of NO_x with ethene as reducing species in oxidant atmosphere, pursuing our work in this field.

2. Experimental description

2.1. Material preparation

Modified silicas with Al (SA), Ti (ST), and Zr (SZ) were synthesized via sol–gel route from molecular precursors using pure grade reagents from Fluka and Merck-Schuchardt. Tetraethyl orthosilane, $Si(OC_2H_5)_4$ (TEOS), aluminium triisopropylate, $Al(OC_3H_7)_3$, tetraethyl orthotitanate, $OC_2H_5)_4$, and zirconium propoxide $Zr(OC_3H_7)_4$ (solution 70% in propanol) were used as source of Si, Al, Ti, and Zr, respectively. Base-catalyzed hydrolysis of TEOS, for SA, and ST, and acid-catalyzed hydrolysis, for SZ, were used for the material synthesis. Detailed information on the procedure of preparation, gelling agent and reagent concentration used could be found in Ref. 34. For comparative purposes, a commercial silica–alumina from Grace Davison, Worms (SAG) was utilized, too. All the oxide materials contained an amount of co-oxide (Al_2O_3, TiO_2, and ZrO_2) in the 12–14 wt% range, as determined from ICP analysis.

The CuO deposition on the synthesized mixed oxides was performed by adsorption method gently dropping a 0.05 M copper acetate ($Cu(C_2H_3O_2)_2$) solution into the slurry of the oxidic material in water (0.073 g_{Cu}/g_{oxide}) thoroughly maintained at 40 °C and pH = 8 by NH_4OH addition. The operation lasted about 1 h. The suspension was maintained at 40 °C for 24 h under stirring, then it rested at room temperature for 18 h. After filtration, the product was thoroughly washed with distilled water, controlling the absence of $Cu(C_2H_3O_2)_2$ in the filtrate by spectrophotometric analysis (λ = 768 nm). All the obtained powders were dried at 120 °C for 12 h and then calcined at 500 °C for 4 h. The catalysts prepared (labelled as Cu/SAG, Cu/SA, Cu/ST, Cu/SZ) contained similar amount of CuO, about 9 wt%.

2.2. Material characterization

The copper content in the samples was established by atomic absorption spectrometry analysis (AA) with a Perkin Elmer 400 spectrometer at λ = 324.8 nm, after dissolution in HNO_3.

X-ray diffraction spectra (XRD) of the powders were collected using a Philips PW 1710 using Cu radiation (K_α = 1.5418 Å) and a Ni filter.

The nitrogen (99.9995% purity) adsorption/desorption isotherms were collected at −196°C using a Sorptomatic 1900 version instrument from Thermofinnigan. Prior to the analysis, the samples were outgassed at 350 °C for 16 h under vacuum. The surface area was calculated using the BET equation (N_2 molecular area = 16.2 $Å^2$). The adsorbed volume, expressed in cm^3 (STP) g^{-1}, was converted into pore volume, cm^3 g^{-1}, using the density of N_2 in the normal liquid state (ρ = 0.8081 g cm^{-3}). Pore volume distribution was calculated from the desorption branch of the isotherm using the Barrett Joyner Halenda (BJH) model equation [35].

Scanning electron micrographs (SEM) were obtained with a JEOL JSM-5500LV instrument. The samples were analysed under moderate vacuum (0.15 Torr) without gold coating. Semi quantitative EDS analysis was performed with X-ray energy of 20 kV.

X-ray photoelectron spectroscopy (XPS) measurements were conducted employing an M-Probe apparatus (Surface Science Instruments) which provided monochromatic Al K_α radiation (1486.60 eV) under a residual pressure of 5×10^{-9} mbar. A spot size of 400×1000 μm with a pass energy of 150 eV was used for the survey spectra, while for the single region acquisition a spot size of 200×750 μm and a pass energy of 25 eV with 0.74 eV resolution were used. The 1s level of hydrocarbon contaminant carbon (284.60 eV) was used as internal reference. The quantitative analysis was performed using the sensitivity factors given by Scofield [36] from the intensities of Cu $2p_{3/2}$, Si 2s, Al 2p, Ti $2p_{3/2}$, and Zr 3d. The XPS peaks were decomposed using a peak-fitting routine. The lines used in the fitting of a peak envelope are defined according to their centered position, half-width, shape (Gaussian or Lorentzian distribution), and intensity. The best fit of the experimental curve by a tentative combination of bands was searched.

Temperature programmed reduction and oxidation experiments were performed using a TPD/R/O-1100 instrument (Thermofinnigan). Redox cycles (TPR/TPO) were realized carrying out in sequence a temperature programmed reduction (TPR) on oxidized sample followed by temperature programmed oxidation (TPO) analysis. The samples were initially pre-treated in air flow (45 ml/min) at 350 °C for 60 min. After cooling to room temperature, the H_2/Ar (4.98% v/v) reducing mixture flowed through the sample at 15 ml/min when the temperature increased from 40 to 900 °C at a rate of 8 °C/min. TPO run was carried out on the reduced sample cooled at 40 °C in H_2Ar flow. After Ar purge (10 ml/min), the O_2/He (1.1% v/v) oxidizing mixture flowed at 15 ml/min through the sample with similar

experimental conditions, in terms of temperature increasing and range, of those used for TPR analysis.

The weighted samples (0.05 g) introduced in the reactor contained amount of reducible CuO in order to obtain K and P values [37] of 100 s and 12 °C, respectively. The H_2 or O_2 consumption was detected by a thermal conductivity detector (TCD). Peak areas were calibrated with pure H_2 or O_2 injections (Sapio, Italy; 99.99999% purity). Deconvolution of the experimental TPR curves was performed by the PeakFit-v4 routine (SeaSolve Software Inc.) searching for the optimum combination of Lorentzian and Gaussian bands.

2.3. Activity in NO_x reduction

Reaction tests of NO_x reduction by ethene in oxidant atmosphere ($NO–C_2H_4–O_2$) under lean conditions were performed in a quartz tubular micro reactor (5 mm ID).

Two types of tests were realized: the first at fixed contact time of 0.360 s and variable temperature (200–450 °C); the second at variable contact time (0.180–0.072 s) and fixed temperature. The mass of catalyst into the reactor ranged from 0.3 g down to 0.13 g (catalyst particles of 0.25–0.35 nm in size) for total flow of the gaseous mixture in the 3–6 Nl/h interval. Catalyst pre-treatment was performed in O_2/He (20% v/v) at 350 °C for 4 h. A set of mass flow controllers (Bronkhorst, Hi-Tec) provided the accurate concentration of the reactant mixture: 1500 ppm of NO, 1500 ppm of C_2H_4, and 30,000 ppm of O_2 in helium. NO_2 besides NO was present in the feed, due to the contemporary presence of NO and O_2 in the gas mixture (typical real concentration: 1300 of NO and 200 of NO_2). The exit gas stream from the reactor flowed through a gas cell (path length 2.4 m multiple reflection gas cell) in the beam of an FTIR spectrometer (Bio-Rad with DTGS detector). The spectrometer response permitted the quantitative analyses of NO (1876 cm^{-1}) and NO_2 (1619 cm^{-1}) for the N-containing species, and of C_2H_4 (951 cm^{-1}), CO (2086 cm^{-1}), and CO_2 (721 cm^{-1}) for the C-containing species. The measurements were carried out each 120 s with accumulation of 19 scans per spectrum and 0.50 cm^{-1}) resolution.

Conversions of NO, NO_2 and C_2H_4 were calculated directly from the experimental absorbances and SCR selectivity (NO_{sx} to N_2) from the competitiveness factor [38].

3. Results and discussion

3.1. Catalyst preparation and characteristics

The morphological properties of the synthesized SA, ST, and SZ mixed oxides and commercial silica–alumina (SAG) are reported in Table 1. All the siliceous oxides are high-surface area materials (surface area values in the 485–777 m^2/g interval) with large pore volumes, in particular SZ. Monomodal pore populations were observed for SA, SAG, and ST (average pore dimension of 3.5, 3.3, and 4.3 nm, respectively) and bimodal for SZ (1.6 and 7.4 nm). The oxide surfaces possessed variable concentration of acid sites which nature, and acid strength depended on co-oxide in the silica structure [32,39]. The number and strength of the surface acid sites were determined from 2-ethyl phenylamine (PEA) desorption by thermogravimetric experiments. The experimental thermograms were interpreted with a computational procedure in order to obtain the fraction of each type of acid site and their distribution on the surface in terms of activation parameters of PEA desorption [34]. Three main types of acid sites were detected on the SA, SAG, ST, and SZ surfaces. The

Table 1
Copper loading and texture characteristics of catalysts

Code	Cu loading			Surface area ($m^2\ g^{-1}$)	Porosity [c] ($cm^3\ g^{-1}$)	B.E.[Cu 2p][d] (eV) and (%)	
	Wt CuO (%)	Molar content ($mmol_{Cu}\ g_{cat}^{-1}$)	$D_{Cu}^{a,b}$ ($atom_{Cu}\ nm^{-2}$)				
SAG	–	–	–	485	0.79	–	
Cu/SAG	9.0	1.13	1.57	434	1.48	933.46 (79)	936.23 (21)
SA	–	–	–	777	0.85	–	
Cu/SA	8.1	1.02	1.60	385	0.63	933.92 (44)	936.03 (56)
ST	–	–	–	494	0.69	–	–
Cu/ST	7.9	0.99	2.60	230	0.60	–	936.26 (100)
SZ	–	–	–	596	1.69	–	
Cu/SZ	8.6	1.09	2.09	313	1.40	933.81 (58)	936.23 (42)

[a]Copper density calculated as amount of Cu introduced per unit surface.
[b]Theoretical monolayer values [48]: Cu/SAG, 0.12; Cu/SA, 0.07; Cu/ST, 0.10; Cu/SZ, 0.09.
[c]Determined from desorption branch of N_2 adsorption isotherm by BJH model.
[d]Obtained by deconvolution of the XPS band of Cu $2p_{3/2}$. Normalized percent intensity of the bands is indicated in parenthesis.

amount of acid sites in the range of medium–high activation energies (80–180 kJ/mol), which corresponds to medium–high site acid strength, was: 1.40 meq/g for SAG, 1.2 meq/g for SZ, 0.92 meq/g for SA, and 0.87 meq/g for ST. Different acid site strength distributions were observed as a function of the co-oxide nature. The remarkable acidity of the two silico–aluminas (SA and SAG) and silica–zirconia (SZ) was expected on the basis of their large use as acid catalyst and acid support in chemical and petrochemical processes [21,30,32,33].

The copper deposition was performed by adsorption from aqueous solution containing copper precursor salt. The operative conditions adopted during the deposition guaranteed the CuO loading around 9 wt% on the three oxide supports. This led to values of copper density for unit surface (D_{Cu}) ranged from 1.6 to 2.6 $atom_{Cu}/nm^2$ (Table 1) that are well above the monolayer coverage in any case. Completely covered support surfaces with CuO were obtained in any case. The copper deposition on the oxidic supports did not alter the shape of the nitrogen adsorption isotherms of the catalysts compared with those of the relevant supports, a decreasing of the amount of nitrogen adsorbed was observed. This led to an appreciable decreasing of surface area for Cu/SA, Cu/ST, and Cu/SZ, but Cu/SAG which had a surface value lightly lower than the SAG support. The pore volumes of catalysts were moderately lower than those of the supports; in this case too, Cu/SAG had a different behavior (Table 1). SEM images revealed completely CuO covered surfaces. By performing several EDS analyses in different points of the samples, it was possible to semi-quantitatively determine the CuO amount. The analyses gave more or less reproducible values as a function of the support nature, suggesting well homogeneous surfaces for Cu/ST and Cu/SZ and more heterogeneous surfaces for Cu/SA and Cu/SAG. The XRD diffraction patterns showed typical profiles of amorphous systems with a very broad band in the 15–30 ° 2θ values, due to disordered Si–OH groups. The 35–38 ° 2θ spectral zone, in which the contribution of the structured CuO phase was expected, was completely flat suggesting the presence of CuO aggregates of dimensions around 10 nm or lower. TEM experiments are in progress to confirm these findings.

The XPS analysis confirmed the exclusive presence of Cu(II) species on all the catalyst surfaces. The bands presented clear spin–orbit split Cu $2p_{1/2}$ and Cu $2p_{3/2}$ peaks along with their shake-up satellites which are known to be characteristics of Cu(II) systems [21,40]. The measured binding energies for the Cu 2p species associated with electron ejection from $2p_{3/2}$ atomic orbital are collected in Table 1. Convoluted XPS bands, in which two contributions of the Cu $2p_{3/2}$ peak at about 934 and 936 eV could be recognized, were observed on the Cu/SA, Cu/SAG, and Cu/SZ surfaces. On Cu/ST, only the high energy peak was detected. The low energy peak (934 eV) can be associated with CuO while the high energy peak can be indicative of a charge transfer from the metal ion toward the support oxide [41]. In any case, CuO species in different local coordination with the support oxidic centers could be pictured. The relative intensity of the low- and high energy peaks is different for the four copper surfaces as clearly emerges from the integration of the deconvolved peaks. The normalized percent intensity for the 934 and 936 eV peaks is reported in Table 1 for all the catalysts. The highest surface presence of CuO-like species was observed on Cu/SAG. On the opposite, CuO species interacting with the support is observed on Cu/ST sample.

The reduction and reoxidation properties of the copper phase of the four catalysts examined were evaluated in TPR and successive TPO experiments. Table 2 summarizes the results obtained in terms of maximum temperatures (T_{max}) and shoulders (T_{sh}) of the reduction (TPR) and oxidation (TPO) peaks. In Table 2 are also reported the CuO reduction (Red_{tot}) and Cu oxidation (OX_{tot}) extents, calculated on the basis of hydrogen and oxygen consumption during the TPR and TPO analyses, respectively. Comparing the reduction profiles of the catalysts, it emerges that only Cu/ST showed a unique reduction peak centered at 239 °C while more complex reduction profiles were obtained for

Table 2
Reduction and oxidation results of CuO-based catalysts from TPR and TPO analysis

Code	TPR											TPO		
	Experimental			Calculated								Experimental		
	T(°C)		(%)	T(°C)				(%)				T(°C)		(%)
	T_{max}	T_{sh}	Red_{tot}	T_1	T_2	T_3	T_4	Red_1	Red_2	Red_3	Red_4	$T_{max,1}$	$T_{max,2}$	Ox_{tot}
Cu/SAG	283 326		90	279	324	–	–	44	46	–	–	193	275	61
Cu/SA	227	262, 308	83	226	257	302	385	20	23	24	16	162	267	63
Cu/ST	239		91	237	311	–	–	75	16	–	–	160	283	40
Cu/SZ	253	327, 428	88	252	314	422	–	54	15	19	–	149	241	50

the catalysts supported on the most acidic supports (SAG, SA, and SZ) with temperatures of reduction in the 230–280 °C and 300–320 °C intervals. Percent of reduction gave values within 90–100%, in any case (Table 2). As a general trend, the CuO deposited on the modified silica supports constituted an easily reducible phase, independently of the nature and dimension of the CuO aggregates. On the basis of a previous TPR investigation on CuO catalysts deposited at various loading (0.3–15 wt% CuO) on SAG [21], the peaks of reduction with temperatures lower than 350 °C could be assigned to dispersed and bulk CuO species (Figure 1 (a–d)). The lack of reduction peaks with T_{max} values lower than 200 °C indicated absence of oxocations $(Cu–O–Cu)^{2+}$, while the presence of peaks with T_{max} higher than 350 °C could indicate the presence of stable copper compounds formed by interaction with surface species of the support.

Due to the complex TPR profiles obtained on the various samples, their deconvolution has been pursued in order to better interpret the profiles. The comparison between the experimental and the deconvoluted TPR bands is shown in Figure 1 (a–d); the maximum temperatures of the calculated peaks together with their percent relative intensities are reported in Table 2. The calculated reduction profiles for the two silico–aluminas (SA and SAG) were well different between each other, in terms of T_{max} values and linewidths. For Cu/SAG, two well distinguished peaks of similar intensity and for Cu/SA, four peaks with very different linewidths could be calculated. A set of three peaks described the experimental profile of Cu/SZ, while quite an unique peak reproduced the experimental reduction profile of Cu/ST. The reduction of the copper phase on the sol–gel prepared supports of high acidity (SA and SZ) showed low defined and very broadened TPR peaks at very high temperatures, 385 and 422 °C for Cu/SA and Cu/SZ, respectively (Table 2). The temperature and feature of these peaks suggest that they could be assigned to copper compounds formed by interaction with the support. These compounds were more stable to the reduction than the dispersed CuO species. Moreover, when a red–ox cycle was applied to Cu/SA (carrying out TPR, TPO, and TPR(2) analyses in sequence), the second reduction profile collected, TPR(2), showed absence of the reduction peak at high temperature (385 °C). This suggests that the peak could not be assigned to CuO species but, more appropriately, to copper containing compounds formed during the copper deposition onto the support that, once reduced, could not be reformed.

The reoxidation of the copper phase created in the first TPR analysis was accomplished under programmed temperature in oxygen flowing (TPO). All the studied catalysts could be completely reoxidized to CuO as indicated by the high values of percent oxidation calculated (Table 2). Quite the same TPO profiles were observed for all the catalysts with $T_{max.1}$ in the 150–190 °C range and $T_{max.2}$ in the 240–280 °C range. The observed results suggest that the oxidation reaction of Cu to CuO proceeded in two steps: at first, an oxidation of dispersed copper species and at higher temperature, the occurrence of bulk oxidation.

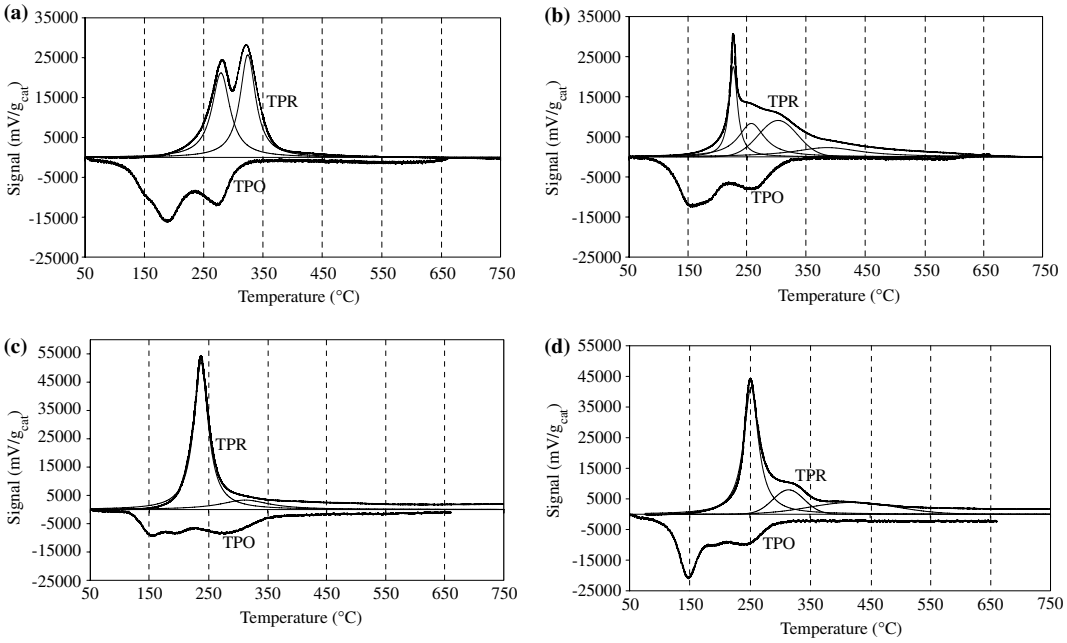

Figure 1. Profiles of reduction (TPR) and oxidation (TPO) at programmed temperature against temperature for Cu/SAG (a), Cu/SA (b), Cu/ST (c), and Cu/SZ (d). Experimental TPR curve, bold line, and deconvoluted peaks, light lines.

3.2. Activity in NO_x reduction

The CuO-based catalysts have been tested in the selective reduction of NO_x with ethene, used as reducing species, in oxidant atmosphere, pursuing the experimental activity performed on other series of copper based catalysts dispersed on supports of various nature and structure [20–46]. Two different kinds of experiments were done; the first at fixed contact time of 0.360 s and variable temperature, in the 200–450 °C interval, and the second at variable contact time, in the 0.180–0.072 s interval, and fixed temperature correspondent to that of maximum NO_x conversion, individuated in the first tests. The contemporary presence in the feed mixture of NO with high O_2 amount, caused that the feed was in fact constituted of both NO and NO_2 (NO_x mixture). Table 3 collects the main results obtained on the four studied catalysts in terms of NO, NO_2, and C_2H_4 conversion for different contact times at constant temperature. For all the catalysts, the trends of the different species analyzed as a function of reaction temperature were in agreement with what already observed over similar copper catalysts [20,21,46]. Conversion of NO_x to N_2 attained a maximum for temperatures around 300 °C (for Cu/ST) or 350 °C (for Cu/SAG, Cu/SA, and Cu/SZ) and then lightly decreased for higher temperatures. The behavior is imputable to the fast consumption of the C_2H_4 reducing species by O_2 combustion which removed C_2H_4 from the reactants preventing further NO_x reduction. According to the previous kinetic interpretation of this reaction over similar catalysts [21,45], NO_x and O_2 compete for the C_2H_4 oxidation. At low temperatures, the kinetics of C_2H_4 combustion by O_2 is slower than that by NO_x, while an opposite trend is observed for higher temperatures. Cu/ST was able to completely oxidize C_2H_4 at lower temperatures than the other catalysts, therefore, the maximum conversion of NO_x to N_2 for Cu/ST was shifted at lower temperature than that observed over Cu/SAG, Cu/SA, and Cu/SZ. Total C_2H_4 conversion was observed over all the three catalysts at temperatures in the 375 and 425 °C interval. C_2H_4 was mainly converted to CO_2 with typical S-shaped curves as a function of temperature. The formation of CO was less than 10–15% in any case and it fell down to zero for temperatures higher than 350 °C. The Cu/SAG, Cu/SA, and Cu/SZ samples showed higher NO_x and C_2H_4 conversions than Cu/ST at any contact time used (Table 3). Conversion of NO_2 was always very higher than that of NO, indicating that NO_2 is more able than NO to interact with the surface CuO phase to create nitrite/nitrate species that successively can evolve into the final product (N_2). However, the NO and NO_2 exit concentrations ran parallel as a function of time/temperature passing through a minimum concentration, corresponding to the formation of maximum N_2 concentration.

Table 3
Catalytic results at variable contact times

Code	Contact time (s)	Conversion[a] (%)		
		NO	NO_2	C_2H_4
Cu/SAG	0.360	20.51	53.64	76.16
	0.180	18.33	46.98	65.66
	0.103	13.62	38.78	43.05
	0.072	12.73	38.56	32.19
Cu/SA	0.360	15.07	54.18	89.61
	0.180	11.19	47.29	79.59
	0.103	10.95	40.60	53.29
	0.072	9.67	34.04	40.62
Cu/ST	0.360	6.67	31.14	53.21
	0.180	5.52	24.35	32.57
	0.103	2.71	18.52	19.26
	0.072	2.11	20.30	14.87
Cu/SZ	0.360	20.81	55.41	77.07
	0.180	17.37	44.99	63.95
	0.103	11.36	35.57	40.39
	0.072	9.45	32.39	28.90

[a]Calculated at the temperature of 350 °C for Cu/SAG, Cu/SA, and Cu/SZ and 300 °C for Cu/ST.

Figure 2 reports the data collected at contact time of 0.36 s and temperatures from 200 to 450 °C plotted as NO_x conversion to N_2 as a function of C_2H_4 conversion to CO_2, considered as an index of the extent of reaction [47]. CO_2 is indeed the common reaction product deriving both from the reduction of NO_x by C_2H_4 and from the oxidation of C_2H_4 by O_2. In this representation, the most active and selective catalysts would have the curves with the highest slopes, reflecting high N_2 formation and low CO_2 production by O_2 combustion. On the contrary, the least active and selective catalysts would have curves with the lowest slopes, reaching high CO_2 production with low N_2 formation. The curves of Cu/SZ, Cu/SAG, and Cu/SA lie almost together, even if it is possible to recognize Cu/SZ as the most active and selective catalyst. On the opposite, the curve of Cu/ST is well apart from the others, indicating the poor ability of this catalyst towards reduction of NO_x.

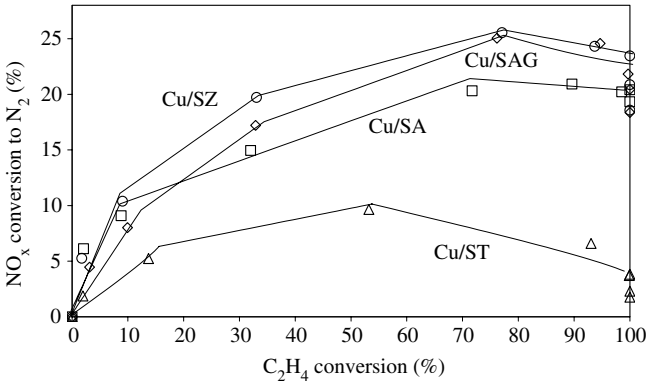

Figure 2. Conversion of NO_x to N_2 as a function of C_2H_4 conversion in the C_2H_4-SCR reaction realized at 0.36 s over the CuO-based catalysts. Each marker corresponds to different reaction temperatures in the range 200–450 °C interval.

The results obtained at decreasing contact times (from 0.36 down to 0.072 s corresponding about to 10,000–50,000 h^{-1} interval) are interesting as represent more reliable conditions from an applicative point of view. As expected, the NO, NO_2, C_2H_4 conversions decreased with decreasing contact time. However, the C_2H_4 conversion decrease was more important than that observed for NO and NO_2. This had a following down on the selectivity of the reaction (SCR selectivity) through the so called competitive factor [38]. This factor gives a measure of the ability of the hydrocarbon reducing species to be oxidized by NO_x rather than by O_2. Figure 3 shows the trend of the calculated reaction selectivity as a function of reaction rate, calculated in terms of rate of N_2 formation. The curves were drawn starting from the data of conversion of NO_x to N_2 before the attainment of the maximum (that is, 300 °C for Cu/ST, 350 °C for Cu/SAG and Cu/SZ, and 375 °C for Cu/SA). As expected, decreasing curves were observed in all cases. The very

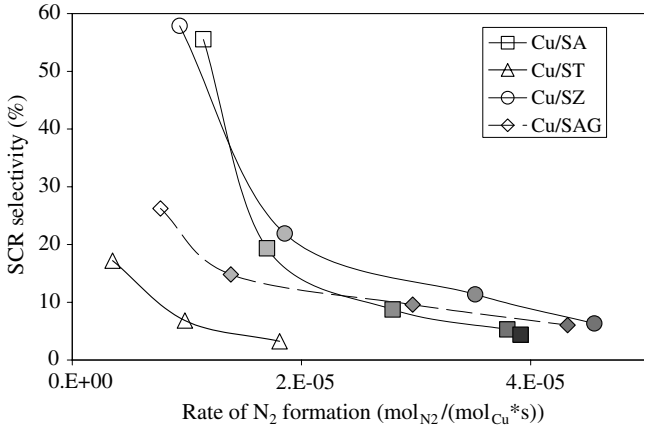

Figure 3. Selectivity of the C_2H_4-SCR reaction, calculated in terms of competitive factor, against rate of N_2 formation. Each curve contains markers corresponding to different temperatures indicated with darker colour tonality with increasing temperature (200, 250, 300, 350, and 375 °C).

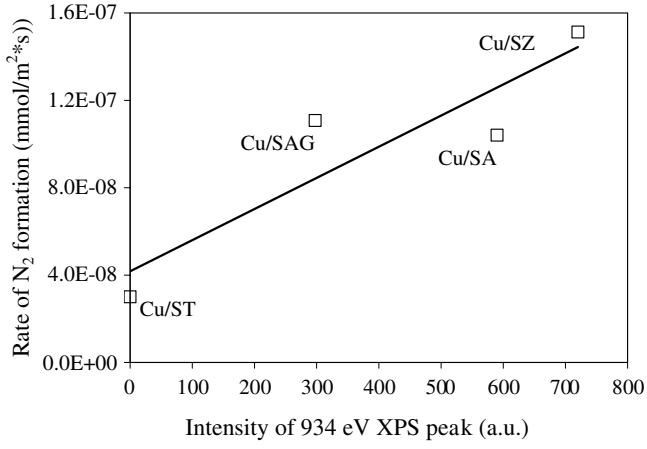

Figure 4. Influence of the intensity of the Cu-XPS peak at 934 eV on the rate of N_2 formation, calculated at 375 °C.

higher values of selectivity observed at low rate of N_2 formation (that is low reaction temperature, 200—250 °C) for Cu/SA and Cu/SZ than those for Cu/SAG and Cu/ST, indicate a better SCR selectivity of the CuO phases supported on the most acidic sol-gel prepared supports. CuO phase on the low acidic support (ST) has very low SCR activity and selectivity (Table 3 and fig. 3), while the CuO deposited on the commercial silico–alumina (SAG) has high SCR activity (high NO_x conversion to N_2) but more modest SCR selectivity.

4. Concluding remarks

Different acidic siliceous supports were loaded with similar amount of CuO in nanosized dimensions by the same method of deposition to create active catalytic phases towards selective reduction of NO_x. The deep differences observed among the CuO-based catalysts relating the physico-chemical characteristics and catalytic activity could be ascribed to the support nature and relating properties, i.e., nature of guest atom in the silica structure and surface acidity. The less acidic surface (ST) could offer a more homogeneous support to the CuO phase and therefore it had more homogeneous properties: only one peak of reduction was observed in the TPR experiments and only one Cu-XPS band was observed. On the contrary, when supports with heterogeneous surfaces are concerned, in particular large distribution of number and strength of the acid sites (SAG, SA and SZ), the CuO phase reflected the support heterogeneity displaying heterogeneous CuO phases: more than one peak of reduction was observed and two contributions in the Cu-XPS bands could be recognized. The dispersion, dimensions, electronic and coordination properties of the CuO aggregates influenced the red–ox characteristics of the copper phase, as observed comparing the TPR profiles that were very different for the different supports.

The observed differences of CuO properties influenced the catalytic activity, too. Figure 4 shows the trend observed when plotting the rate of N_2 formation as a function of the intensity of the Cu-XPS peak at 934 eV, typical of CuO species, for each catalyst. As higher the intensity of the XPS was as higher the rate of N_2 formation was observed. This indicates the important role of the electronic structure of the CuO species on the catalytic activity.

Acknowledgment

Authors wish to thank Prof. Vittorio Ragaini for the encouragements had during this research and Dr. Italo Campostrini for his kindness in doing the SEM-EDS measurements.

References

[1] R. Prasad, L.A. Kennedy and E. Ruckenstein, Catal. Rev.-Sci. Eng. 26 (1984) 1.

[2] M.F.M. Zwinkels, S.G. Järås, P.G. Menon and T.A. Griffin, Catal. Rev.-Sci. Eng. 35 (1993) 319.
[3] F. Kapteijn, S. Stegenga, N.J.J. Dekker, J.W. Bijsterbosch and J.A. Moulijn, Catal. Today 16 (1993) 273.
[4] H. Hamada, Catal. Today 22 (1994) 21.
[5] K.A. Bethke, M.C. Kung, B. Yang, M. Shah, D. Alt, C. Li and H.H. Kung, Catal. Today 26 (1995) 169.
[6] A.Q.M. Boon, F. van Looij and J.W. Geus, J. Mol. Catal. 75 (1992) 277.
[7] P. Larsson and A. Andersson, J. Catal. 179 (1998) 72.
[8] A. Martinez-Arias, M. Fernandez-Garcia, O. Galvez, J.M. Coronado, J.A. Anderson, J.C. Conesa, J. Soria and G. Munuera, J. Catal. 195 (2000) 207.
[9] P. Subbanna, H. Greene and F. Desal, Environ. Sci. Technol. 22 (1998) 557.
[10] U.S. Ozkan, R.F. Kueller and E. Moctezuma, Ind. Eng. Chem. Res. 29 (1990) 1136.
[11] H. Rajesh and U.S. Ozkan, Ind. Eng. Chem. Res. 32 (1993) 1622.
[12] O.V. Komova, A.V. Simakov, L.T. Tzykoza, N.N. Sazonova, A.V. Ushakov, G.B. Barannik and Z.R. Ismagilov, React. Kinet. Catal. Lett. 54 (1995) 361.
[13] G. Centi, C. Nigro, S. Perathoner and G. Stella, Catal. Today 17 (1993) 159.
[14] G. Centi and S. Perathoner, Appl. Catal. A 132 (1995) 179.
[15] A. Dandekar and M.A. Vannice, Appl. Catal. B 22 (1999) 179.
[16] M. Matsuoka, W. Ju, K. Takahashi, H. Yamashita and M. Anpo, J. Phys. Chem. B 104 (2000) 4911.
[17] H. Praliaud, S. Mikhailenko, Z. Chajar and M. Primet, Appl. Catal. B 16 (1998) 359.
[18] F. Radtke, R.A. Koeppel, E.G. Minardi and A. Baiker, J. Catal. 167 (1997) 127.
[19] L. Chen, T. Horiuchi, T. Osaki and T. Mori, Appl. Catal. B 23 (1999) 259.
[20] P. Carniti, A. Gervasini, V.H. Modica and N. Ravasio, Appl. Catal. B 28 (2000) 175.
[21] S. Bennici, A. Gervasini, N. Ravasio and F. Zaccheria, J. Phys. Chem. B 107 (2003) 5168.
[22] J.A. Schwarz, C. Contescu and A. Contescu, Chem. Rev. 95 (1995) 477.
[23] F. Pinna, Catal. Today 41 (1998) 129.
[24] V. Indovina, M. Occhiuzzi, D. Pietrogiacomi and S. Tuti, J. Phys. Chem. B 103 (1999) 9967.
[25] C. Márquez-Alvarez, I. Rodríguez-Ramos, A. Guerrero-Ruiz, G.L. Haller and M. Fernández-García, J. Am. Chem. Soc. 119 (1997) 2905.
[26] J.A. Schwarz, Chem. Rev. 95 (1995) 477.
[27] D.R. Ulrich, Chemtech (1988) 242.
[28] S. Ebener and W. Winter, J. Eur. Ceram. Soc. 16 (1996) 1179.
[29] D. Enache, M. Roy-Auberger, K. Esterle and R. Revel, Colloids Surf. A: Physicochem. Eng. Aspects 220 (2003) 223.
[30] C. Flego, L. Carluccio, C. Rizzo and C. Perego, Catal. Commun. 2 (2001) 43.
[31] A. Carati, G. Ferraris, M. Guidotti, G. Moretti, R. Psaro and C. Rizzo, Catal. Today 77 (2003) 315.
[32] A. Corma, Chem. Rev. 95 (1995) 559.
[33] J.M. Miller and L.J. Lakshmi, Appl. Catal. A 190 (2000) 197.
[34] P. Carniti, A. Gervasini and S. Bennici, J. Phys. Chem., submitted.
[35] E.P. Barrett, L.G. Joyner and P. Halenda, J. Am. Chem. Soc. 73 (1951) 373.
[36] J.H. Scofield, J. Elect. Spect. Relat. Phenom. 8 (1976) 129.
[37] P. Malet and A. Caballero, J. Chem. Soc., Faraday Trans. 184 (1988) 2369.
[38] K.A. Bethke, M.C. Kung, B. Yang, M. Shah, D. Alt, C. Li and H.H. Kung, Catal. Today 169 (1995) 26.
[39] K. Tanabe in: Solid Acid and Base Catalysts:Catalysis Science and Technology, J.R. Anderson and M. Boudart (eds.), Vol. 2 (Springer, Berlin, 1981), Ch. 5, p. 231.
[40] J.P. Espinós, J. Morales, A. Barranco, A. Caballero, J.P. Holgado and A.R. González-Elipe, J. Phys. Chem. B 106 (2002) 6291.
[41] A. Auroux, A. Gervasini and C. Guimon, J. Phys. Chem. B 103 (1999) 7195.
[42] A. Auroux, C. Picciau and A. Gervasini in: Porous Materials in Environmentally Friendly Processes, Stud. Surf. Sci. Catal., I. Kiricsi, G. Pail-Borbély, J.B. Nagy and H.G. Karge (eds), Vol. 125 (Elsevier, Amsterdam, 1999), p. 555.
[43] A. Gervasini, C. Picciau and A. Auroux, Micropor. Mesopor. Mater. 35 (2000) 457.
[44] A. Gervasini and A. Auroux in: *12th International Congress on Catalysis, Stud. Surf. Sci. Catal., Vol. 130(B)*, A. Corma, F.V. Melo, S. Mendioroz and J.L.G. Fierro (eds.), (Elsevier, Amsterdam, 2000), p. 1253.
[45] A. Gervasini and P. Carniti, Catal. Lett. 84 (2002) 235.
[46] S. Bennici, A. Gervasini and V. Ragaini, Ultrason. Sonochem. 10 (2003) 61.
[47] A. Gervasini, P. Carniti and V. Ragaini, Appl. Catal. B 22 (1999) 201.
[48] H.E. Ries, K.J. Laidler, W.E. Innes, F.G. Ciapetta, C.J. Plank and P.W. Selwood in: *Catalysis. Volume I Fundamental Principles (Part I)*, Paul H. Emmett (ed.), (Book Division Reinhold Publishing Corporation, New York, 1954) p. 258.